

## Article

# Influence of Electrostatic Field on Mixed Aqueous Solution of Calcium and Ferrous Ions: Insights from Molecular Dynamics Simulations

Yong Han <sup>1,2,\*</sup>, Bingjia Wei <sup>2</sup>, Xiaoqiang Guo <sup>2</sup> and Tifeng Jiao <sup>1,\*</sup> 

<sup>1</sup> State Key Laboratory of Metastable Materials Science and Technology, Yanshan University, Qinhuangdao 066004, China

<sup>2</sup> School of Electrical Engineering, Yanshan University, Qinhuangdao 066004, China

\* Correspondence: hanyong@ysu.edu.cn (Y.H.); tfjiao@ysu.edu.cn (T.J.)

**Abstract:** In order to investigate the anti-scaling and anti-corrosion characteristics of an electrostatic anti-fouling system in the application process, the influence of an electrostatic field (EF) on the structure and dynamics of hydrated  $\text{Ca}^{2+}$  and hydrated  $\text{Fe}^{2+}$  in a mixed aqueous system was studied through the calculation and analysis of the radial distribution function (RDF), self-diffusion coefficients, viscosity, and hydrogen bond structure by using molecular dynamics simulation. The study results show that the EF can decrease the radius of the first water shell of hydrated  $\text{Ca}^{2+}$  but increase that of  $\text{Fe}^{2+}$ , which will reduce the possibility of forming calcite. The EF can make water molecules and  $\text{Fe}^{2+}$  more active, which can hinder iron release and thus decrease iron corrosion products. In addition, the EF can enhance the hydrogen structure of water molecules in the aqueous solution.

**Keywords:** electrostatic anti-fouling; calcium carbonate; ferrous ion; corrosion; molecular dynamics; electrostatic field



**Citation:** Han, Y.; Wei, B.; Guo, X.; Jiao, T. Influence of Electrostatic Field on Mixed Aqueous Solution of Calcium and Ferrous Ions: Insights from Molecular Dynamics Simulations. *Coatings* **2022**, *12*, 1165. <https://doi.org/10.3390/coatings12081165>

Received: 28 June 2022

Accepted: 10 August 2022

Published: 12 August 2022

**Publisher's Note:** MDPI stays neutral with regard to jurisdictional claims in published maps and institutional affiliations.



**Copyright:** © 2022 by the authors. Licensee MDPI, Basel, Switzerland. This article is an open access article distributed under the terms and conditions of the Creative Commons Attribution (CC BY) license (<https://creativecommons.org/licenses/by/4.0/>).

## 1. Introduction

Fouling and iron corrosion are common problems in the water industry. Fouling results in degradation in the performance of heat exchangers. Iron corrosion can destroy the pipe and pollute the drinking water due to the suspension of iron particles. An electrostatic anti-fouling (EAF) system is one of the most common and effective ways to solve these problems. Water scale is almost entirely composed of calcium carbonate ( $\text{CaCO}_3$ ), which naturally occurs in six various forms: calcite, aragonite, vaterite, two hydrate phases, and amorphous calcium carbonate (ACC). ACC is perhaps the most vital to growth processes since it can create the precursor to the crystallization of those phases and plays a critical role in the biomineralization process for this substance [1]. Thus, the electric field's impact on calcium carbonate has been the focus of the great majority of studies looking into the anti-fouling mechanism of EAF. It consists of two main aspects: how calcium carbonate crystals are formed and how the structure of scale crystals changes under electric fields. The impact of an electric field on calcium carbonate crystallization was studied by Qi et al. [2]. Their results show that the electric field applied to the  $\text{CaCO}_3$  solution affects the lattice structure and crystal shape of  $\text{CaCO}_3$  crystals. According to Li et al. [3], the scale sample produced by electrostatic water included more aragonite than before. Most equipment in industrial systems is made of carbon steel, and its main chemical composition is iron. Therefore, researchers who investigate the mechanism of metal corrosion tend to use iron as the study object. Lin et al. [4] found that the electric field accelerates steel corrosion, and the electric field favors the generation of plate-shaped  $\gamma\text{-FeOOH}$  and inhibits the formation of  $\alpha\text{-FeOOH}$ . In addition, the scaling of calcium carbonate has a certain influence on iron corrosion. Sarin et al. [5] found that  $\text{CaCO}_3$  plays a role in reducing iron release, which can alleviate water pollution problems, and Harris et al. found that the scaling tendency in

water is the main factor determining the corrosion rate of iron [6]. The different contents of metal cations (including  $\text{Fe}^{2+}$ ) in aqueous solutions also have a certain influence on the precipitation process of  $\text{CaCO}_3$  [7]. Less attention has been paid to the impact of an electrostatic field (EF) on the microcosmic particle structure in aqueous systems.

Due to the relatively poor solubility of calcium carbonate, there are nearly zero  $\text{CO}_3^{2-}$  ions in hard water, but  $\text{HCO}_3^-$  ions are plentiful. As hydrated ions,  $\text{Ca}^{2+}$  and  $\text{Fe}^{2+}$  can be found in aqueous solutions. Additionally, these hydrated ions form hydrogen bonds with additional water molecules [8–10]. The formation, growth, and crystal structure of calcium carbonate precipitates are mainly determined by the structural and dynamic properties of  $\text{Ca}^{2+}$ .  $\text{Fe}^{2+}$  plays an important role in the metal corrosion process. The main reactions of iron corrosion are shown below.

The iron in the material loses two electrons and forms  $\text{Fe}^{2+}$ .



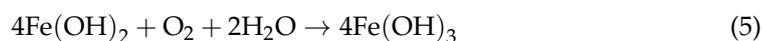
Electron acceptors such as oxygen or hydrogen ions in aqueous solutions serve to complete the reaction.



Ferrous solids such as ferrous hydroxide can form.



$\text{Fe}(\text{OH})_2$  can be further oxidized to  $\text{Fe}(\text{OH})_3$  attached to the wall of the tube.



Therefore, by examining the impact of an EF on the structure and molecular dynamics of hydrated calcium ions and hydrated divalent iron ions, the mechanism of scale inhibition and corrosion under EAF in aqueous solutions may be more readily ascertained. This paper's study involves a blend of  $\text{CaCl}_2$  and  $\text{FeCl}_2$ . The position of the first water shell of calcium ions and divalent iron ions, the framework of hydrated calcium ions and divalent iron ions, the self-diffusion coefficients of calcium ions, divalent iron ions, and water molecules, and hydrogen bonding in the liquid solution were all investigated using MD simulations to study the structural and kinetic properties of aqueous  $\text{CaCl}_2$  solutions under an external EF. It should be noted that although the materials in this study and our previous work [11] are mixed aqueous solutions of two ions containing calcium ions, there are significant differences in the research details between the two. Our previous work mainly focused on the influence of magnesium ion impurities on the scaling process of calcium ions during the operation of the EAF system. However, in this study, we chose to pay attention to the influence of the EAF system on the corrosion process of iron water transmission pipes.

## 2. Model and Simulation Details

An equilibrium MD simulation was performed by using the Gromacs 5.0.2 software [12]. NPT ensembles were used for all simulations. The thermostat was adjusted to 300 K. The pressure was established at  $1.01 \times 10^5$  Pa. As stated in Table 1, four sets of aqueous solution systems were constructed. The  $\text{CaCl}_2$  aqueous solution had a concentration of 4 mol/kg, and there was only a 0.5 percent difference in concentration between models and tests [13]. In our study, the water molecule was represented by the SPCE model. In this simulation, ion–water interactions were simulated using the GROMOS force field [14–16]. A cutoff of 1.2 nm was used for Lennard-Jones interactions, and a real-space cutoff of 1.2 nm was used for electrostatic interactions when using the particle mesh Ewald (PME) [15] technique. Fourier spacing has a value of 0.12 nm. The Lennard-Jones potential

parameters for the particles utilized in the GROMOS force field are shown in Table 2. The Lennard-Jones parameters of  $\text{Fe}^{2+}$  were taken from Fernanda et al. [17]. All of the simulations employed a 2.0 fs time step, and a  $2.5 \times 10^4$  ps simulation time was used to confirm the stability of the system setup. Following a  $1 \times 10^4$  ps period of system equilibration, the structures and characteristics of the sample (apart from the self-diffusion coefficient data) were determined throughout a  $1.5 \times 10^4$  ps period (the final  $1.5 \times 10^4$  ps of each simulation). By computing the average result of  $1.5 \times 10^4$  ps, which was separated into ten segments, the average values of the parameters were acquired. The leapfrog method is a type of integration algorithm used for motion equations. The simulation box measures 4 nm, 4 nm, and 3 nm in length. The EF was  $1 \text{ V}/\mu\text{m}$  in intensity. The EF was used in a certain way (corresponding to the  $y$ -axis). The simulations were run as described in the step above. Previous research has confirmed the accuracy of our MD simulations and error analyses [18].

**Table 1.** Composition of the  $\text{CaCl}_2$  solution studied by Gromacs.

Sample	$[\text{H}_2\text{O}]$	$[\text{Fe}^{2+}]$	$[\text{Ca}^{2+}]$	$[\text{Cl}^-]$	[Total]
0F	1110	0	80	160	1350
10F	1110	10	80	180	1380
20F	1110	20	80	200	1410
30F	1110	30	80	220	1440

NOTE: “0F” indicates no  $\text{Fe}^{2+}$  ions were added, “10F” indicates 10  $\text{Fe}^{2+}$  were added, “20F” indicates 20  $\text{Fe}^{2+}$  were added, and “30F” indicates 30  $\text{Fe}^{2+}$  were added.

**Table 2.** The MD simulations employed the Lennard-Jones potential parameters according to the combining rules of Lorentz and Berthelot, i.e.,  $\epsilon_{ij} = (\epsilon_{ii}\epsilon_{jj})^{1/2}$ ,  $\sigma_{ij} = (\sigma_{ii} + \sigma_{jj})/2$ .

	$\epsilon_{ii}/(\text{kJ/mol})$	$\sigma_{ii}/\text{nm}$
$\text{Ca}^{2+}$	0.5069	0.2813
$\text{Fe}^{2+}$	$2.135 \times 10^{-6}$	1.9129
$\text{Cl}^-$	1.2889	0.3470
O	1.7250	0.2626

### 3. Results and Discussion

#### 3.1. Structural Parameters

The hydration shell regulates the mobility of ion pairs in the solution and the interaction between ion pairs [19]. A change in the hydration shell can affect calcium carbonate precipitation [20], and the layers of hydration around these ions define the route(s) for crystal formation in aquatic settings [21]. In this segment, the average radii of the first water shells of  $\text{Ca}^{2+}$  ( $R_{\text{Ca-O}}$ ),  $\text{Fe}^{2+}$  ( $R_{\text{Fe-O}}$ ),  $\text{Ca}^{2+}$  ( $n_{\text{Ca-O}}$ ),  $\text{Fe}^{2+}$  ( $n_{\text{Fe-O}}$ ),  $\text{Ca}^{2+}$  ( $n_{\text{Ca-O}}$ ), and  $\text{Fe}^{2+}$  ( $n_{\text{Fe-O}}$ ) under an external EF and under no EF are provided.

It is possible to determine  $R_{\text{Ca-O}}$  and  $R_{\text{Fe-O}}$  from the RDF  $[g(r)]$ ;  $[g(r)]$  [22] is calculated as shown in Equation (6):

$$g_{AB}(r) = \frac{\langle \rho_B(r) \rangle}{\langle \rho_B \rangle_{\text{local}}} = \frac{1}{\langle \rho_B \rangle_{\text{local}}} \frac{1}{N_A} \sum_{i \in A} \sum_{j \in B} \frac{\delta(r_{ij} - r)}{4\pi r^2} \quad (6)$$

where  $\langle \rho_B(r) \rangle$  is the particle density of particle  $B$  on all spheres surrounding particle  $A$  with radius  $r_{\text{max}}$ ,  $\langle \rho_B \rangle_{\text{local}}$  is the particle density of particle  $B$  at distance  $r$  around particle  $A$ ,  $N_A$  denotes the number of particles  $A$ , and  $N_B$  denotes the number of particles  $B$ . Typically,  $r_{\text{max}}$  has a value equal to half of the box's minimum length.

The values of  $n_{\text{Ca-O}}$  and  $n_{\text{Fe-O}}$  are calculated using Equation (7) [14]:

$$n_{\text{Ca}}^{\text{O}}(r_s) = 4\pi\rho_0 \int_0^{r_s} g_{\text{CaO}}(r)r^2 dr \quad (7)$$

For  $n_{\text{Ca-O}}$ ,  $r_s$  is the location of the first local minimum of  $g_{\text{CaO}}(r)$ , which is also the location of  $R_{\text{Ca-O}}$ ; for  $n_{\text{Fe-O}}$ ,  $r_s$  is the location of the first local minimum of  $g_{\text{FeO}}(r)$ , which is also the location of  $R_{\text{Fe-O}}$ .

Figure 1 shows RDFs and the corresponding running integration number of the  $\text{CaCl}_2$  solution containing different numbers of  $\text{Fe}^{2+}$ . The coordinates of the first peak in  $g_{\text{CaO}}(r)$ , the coordinates of the first peak in  $g_{\text{FeO}}(r)$ ,  $R_{\text{Ca-O}}$ ,  $R_{\text{Fe-O}}$ ,  $n_{\text{Fe-O}}$  and  $n_{\text{Ca-O}}$  are presented.

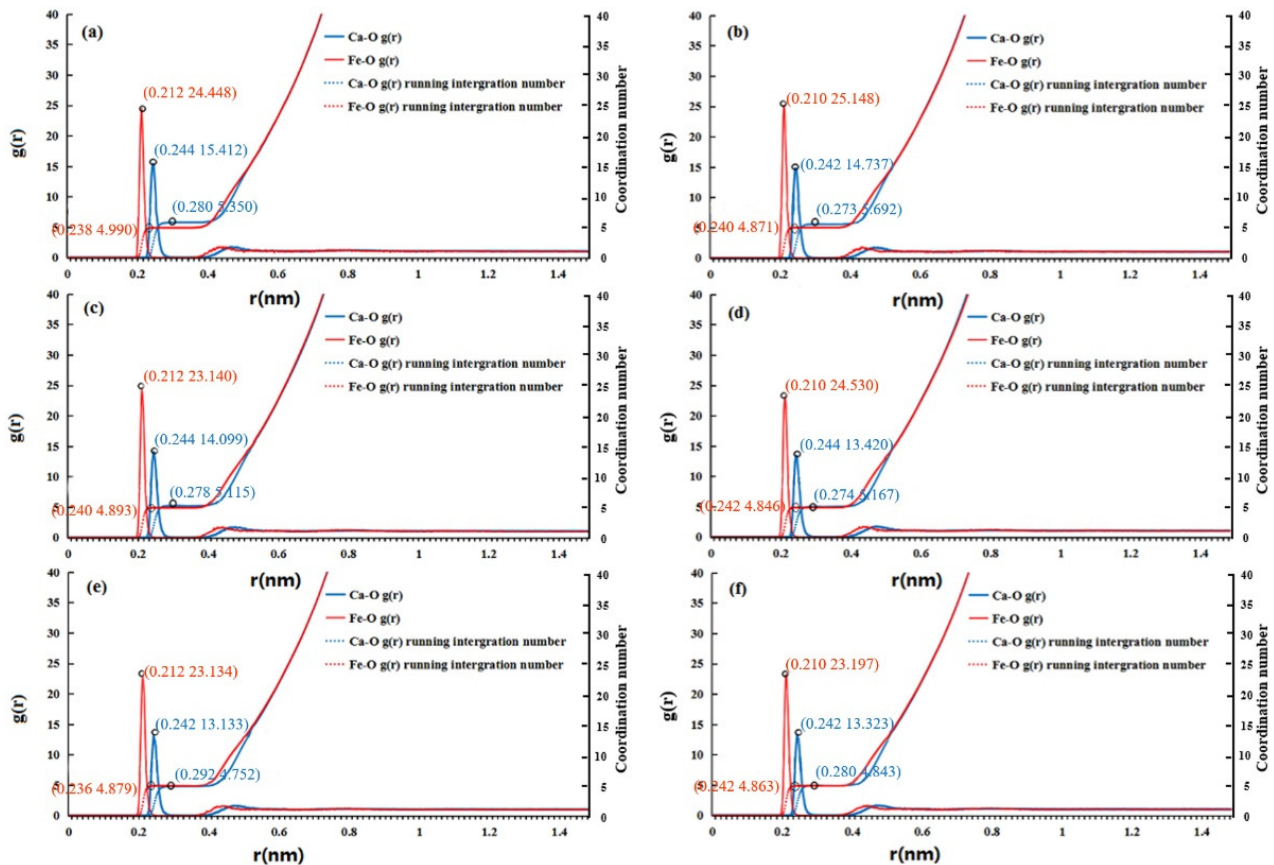


**Figure 1.** RDFs (curves with one obvious peak) and corresponding running integration numbers (single increment curves) of  $\text{CaCl}_2$  solution containing different numbers of  $\text{Fe}^{2+}$  with an electric field applied (b,d,f) or without an electric field (a,c,e): (a,b) 10  $\text{Fe}^{2+}$  added, (c,d) 20  $\text{Fe}^{2+}$  added, and (e,f) 30  $\text{Fe}^{2+}$  added.

According to Figure 1a,c,e, it can be seen that the height of the first peak in  $\text{Fe}^{2+}\text{-O } g(r)$  is higher than its  $\text{Ca}^{2+}\text{-O } g(r)$  counterpart. The first peak position of  $\text{Fe}^{2+}\text{-O } g(r)$  is less than the first peak position of  $\text{Ca}^{2+}\text{-O } g(r)$ , which implies that  $\text{Fe}^{2+}$  has a smaller size than  $\text{Ca}^{2+}$ , and the hydrated structure of  $\text{Fe}^{2+}$  is more stable than  $\text{Ca}^{2+}$  [23]. Furthermore, the higher the content of  $\text{Fe}^{2+}$  ions, the lower the heights of the first peak in  $\text{Ca}^{2+}\text{-O } g(r)$ .  $\text{Fe}^{2+}$  was added, but it had no discernible impact on  $R_{\text{Ca-O}}$ . With an increase in the amount of  $\text{Fe}^{2+}$  supplied, the  $n_{\text{Ca-O}}$  drops. The decrease in  $n_{\text{Ca-O}}$  could be due to the more stable hydrated structure of  $\text{Fe}^{2+}$  compared to  $\text{Ca}^{2+}$ , which means that fewer water molecules remain in the water shell of  $\text{Ca}^{2+}$ . In the  $\text{CaCl}_2$  solution containing  $\text{Fe}^{2+}$  under an EF, Figure 1b,d,f demonstrate that the values of  $R_{\text{Ca-O}}$  decrease while the values of  $n_{\text{Ca-O}}$  increase, which is consistent with our earlier research on “pure”  $\text{CaCl}_2$  aqueous solutions [24]. This is because the average binding ability of water molecules increases monotonically as the hydration shell becomes smaller [25,26]. In addition, the larger height and sharpness of the ferrous peak suggest a more stable structure under the EF, which means that the EF can make the  $\text{Fe}^{2+}$  radius smaller. The enthalpy of formation of ACC clusters decreases as the coordination number increases in the first hydration shell of  $\text{Ca}^{2+}$ , and the stability of

ACC correlates with water content. Experimentally, it has been proposed that “transient” ACC is largely anhydrous, while “stable” ACC contains some water [20]. Therefore, the EF increases the coordination number in the first hydration shell of  $\text{Ca}^{2+}$  and decreases the enthalpy of ACC, which can enhance the stability of ACC. To a certain extent, the EF reduces the possibility of ACC converting to calcite by changing the structure of the first hydration shell of  $\text{Ca}^{2+}$ , which will play a role in scale inhibition (according to our previous study [27]). The creation of carbonate ions close to  $\text{Ca}^{2+}$  is made easier by the reduced radius of the initial water shell of  $\text{Ca}^{2+}$ , which promotes the development of calcium carbonate crystals [24].

Figure 1 shows that the values of  $R_{\text{Fe-O}}$  range between 0.230 and 0.240 nm, and the values of  $n_{\text{Fe-O}}$  are distributed between 4.800 and 5.000, which is consistent with the results reported in Reference [28]. In  $\text{CaCl}_2$  solution under an EF, the values of  $R_{\text{Fe-O}}$  are larger, and the values of  $n_{\text{Fe-O}}$  are lower. According to experimental findings [29], this suggests that the EF decreases hydration between  $\text{Fe}^{2+}$  and water molecules.

In addition, we also calculated the RDF of chloride ions around  $\text{Ca}^{2+}$  and  $\text{Fe}^{2+}$  under an EF (not shown here). The calculation results show that although the influence of the EF on the distribution of chloride ions around cations is small, it enhances the interaction between cations and anions (the number of anions around cations increases slightly). This is consistent with the conclusion of our previous paper. Therefore, the distribution of chloride ions is not analyzed in detail in this section.

### 3.2. Self-Diffusion Coefficients of $\text{Ca}^{2+}$ and $\text{Fe}^{2+}$ and Water Molecule

This section examines  $\text{Ca}^{2+}$ ,  $\text{Fe}^{2+}$ , and water molecule self-diffusion coefficients in the presence of an exogenous EF in the  $\text{CaCl}_2$  aqueous solution system. An important factor that may affect the course of chemical reactions in aqueous systems is the self-diffusion coefficient of ions. In addition, the self-diffusion coefficient may change significantly when the structure of the cation or anion is changed or another ion is involved [30]. It is worth noting that, in the simulation model in this paper, the solution seems to be strongly concentrated since there is 4 mol/kg  $\text{CaCl}_2$ , which means 4 mol of  $\text{Ca}^{2+}$  and 8 mol of  $\text{Cl}^-$  dissolved in 55.6 mol of water that solvates them (see Table 1). It may be considered that there are no free water molecules, because all water molecules seem to become ionic coordination water. This may make water molecules lack independent diffusivity. In fact, as the ions move in the water, the coordination water around the ions is not fixed, and they will be constantly replaced by the surrounding water molecules [13]. Therefore, the water molecules in this paper can be considered to have independent diffusivity, but this diffusivity will be affected by ions.

In this research, the “Einstein relation” [31] was used to calculate the self-diffusion coefficients of  $\text{Ca}^{2+}$  ( $D_{\text{Ca}}$ ) and water molecules ( $D_{\text{O}}$ ):

$$D = \lim_{t \rightarrow \infty} \frac{1}{6t} \langle [r_i(t) - r_i(0)]^2 \rangle \quad (8)$$

where  $r_i(0)$  is the starting position, the parentheses represent the set mean, and  $r_i(t)$  is the numerator position  $i$  at time  $t$ . Fitting the slope of the linear component of the mean square displacement (MSD) and dividing by six are the particular steps in computing the self-diffusion coefficient of a particle. The RANSAC algorithm determines the linear component of the MSD. RANSAC is a technique for robust model fitting in the presence of outliers in the data [32].

The impact of  $\text{Fe}^{2+}$  on the values of  $D_{\text{Ca}}$  and  $D_{\text{O}}$  with and without an EF is shown in Table 3. With regard to the self-diffusion coefficient, the standard deviation of the simulation results presented in Table 3 is conservatively estimated to be in the region of 0.41%–5.11%. Table 3 shows that whether or not there is an EF, the values of  $D_{\text{Ca}}$  and  $D_{\text{O}}$  both drop as the amount of  $\text{Fe}^{2+}$  increases. Moreover, the higher the  $\text{Fe}^{2+}$  ion content, the lower the values of  $D_{\text{Ca}}$  and  $D_{\text{O}}$ . In addition, Table 3 shows that the external EF can increase

the values of  $D_{Ca}$  and  $D_o$  no matter how much  $Fe^{2+}$  exists in the  $CaCl_2$  aqueous solution during all simulations.

**Table 3.** The  $10^5$  self-diffusion coefficients of  $Ca^{2+}$  ( $D_{Ca}$ ) and water molecules ( $D_o$ ) with no  $Fe^{2+}$  ions added (0F) and ten  $Fe^{2+}$  added (10F), twenty  $Fe^{2+}$  added (20F), and thirty  $Fe^{2+}$  added (30F) with and without EF.

Sample	Average	St.dev	Average	St.dev
	$10^{-5} \text{ cm}^2 \cdot \text{s}^{-1}$			
	Without Electrostatic Field		Under Electrostatic Field	
$D_{Ca}$				
0F	0.0608	0.0003	0.0707	0.0001
10F	0.0185	0.0005	0.0239	0.0001
20F	0.0124	0.0003	0.0137	0.0007
30F	0.0108	0.0005	0.0128	0.0001
$D_o$				
0F	0.6626	0.0004	0.7276	0.0003
10F	0.1837	0.0004	0.1870	0.0006
20F	0.1573	0.0005	0.1596	0.0001
30F	0.1283	0.0005	0.1343	0.0003
$D_{Fe}$				
10F	0.0188	0.0009	0.0195	0.0004
20F	0.0158	0.0004	0.0180	0.0002
30F	0.0142	0.0002	0.0172	0.0004

The valence and structural order of cations in aquatic environments impact the rate at which water molecules diffuse [33]. According to Table 3, the values of  $D_o$  are  $0.6626 \times 10^{-5} \text{ cm}^2 \cdot \text{s}^{-1}$  and  $0.7276 \times 10^{-5} \text{ cm}^2 \cdot \text{s}^{-1}$  without and with an EF, respectively, when  $Fe^{2+}$  is not in the solutions, in contrast to the values of  $D_o$  in the range of  $0.12 \times 10^{-5} \text{ cm}^2 \cdot \text{s}^{-1}$ – $0.18 \times 10^{-5} \text{ cm}^2 \cdot \text{s}^{-1}$  when different numbers of  $Fe^{2+}$  ions are present. It is worth noting that when iron ions exist, the existence of an electric field can only slightly increase the diffusion coefficient of water molecules (with an increase of about 5%), which may be due to the binding of iron ions to water molecules, weakening the influence of the electric field. Water molecules that are coupled to metal ions are successfully immobilized in relation to the bulk water by being contained in a hydration layer [21]. As a result, when  $Fe^{2+}$  is available in the  $CaCl_2$  solution, its significant capacity to bind to water molecules restricts the activity of the water molecules. The  $D_o$  values decline. The presence of  $Fe^{2+}$  is responsible for the decrease in the self-diffusion coefficient of  $Ca^{2+}$ . The  $CaCl_2$  aqueous solution becomes more compact due to the electrostatic contact between  $Fe^{2+}$  and the water molecule.  $Ca^{2+}$  activity is constrained, and its self-diffusion coefficient is decreased.

The EF lowers the water molecule's self-diffusion coefficient while increasing the hydrogen bond network's binding capacity in pure water solutions [34]. However, the findings in Table 3 demonstrate that for the four example  $CaCl_2$  aqueous solutions, the EF may increase the water molecule's self-diffusion coefficient. Therefore, the rise in the diffusion coefficient of water molecules in aqueous  $CaCl_2$  solutions can be attributed to the activity of metal ions in the solution. When  $Ca^{2+}$  and  $Fe^{2+}$  diffuse, they either displace their solvated shells along their trajectories or break the strong connections with the initial water shell [35]. Thus, the EF increases the activity of  $Ca^{2+}$  and  $Fe^{2+}$  and influences the relatively stable water molecule hydrogen bond network.

As can be seen in Table 3, the self-diffusion coefficients of water molecules and  $Fe^{2+}$  in aqueous  $CaCl_2$  solutions grow in the presence of EF. The speed at which oxidants are transported to the scale's surface may be increased by increasing the activity of water molecules, which can reduce iron release and the amounts of iron corrosion products that dissolve in water [36,37]. Water contamination issues may be resolved. Additionally, the rise in  $D_o$  and  $D_{Fe}$  may indicate that the EF has the ability to accelerate the oxidation of  $Fe^{2+}$ .

### 3.3. Viscosity of the $\text{CaCl}_2$ Aqueous Solution

Generally, the formation of calcium carbonate precipitation involves three stages: nucleation, grain growth, and aggregation of  $\text{CaCO}_3$  crystals [38]. The viscosity of the solution affects the precipitation of calcium carbonate and the corrosion behavior of iron in the solution [39–43]. According to experimental findings, the crystallinity of scale-forming ions mixed with water is inversely related to the viscosity of a liquid [44]. A liquid's dynamic viscosity is another kinetic characteristic that affects how quickly solutes in the liquid alter their conformation. It is susceptible to an EF [44].

The following equation can be used to determine the viscosity ( $\eta$ ):

$$\eta = \frac{A \rho}{V k^2} \quad (9)$$

where  $\rho$  and  $V$  stand for density and velocity, respectively;  $A$  is a constant [44], and we can deduce the following from a cosine that meets both requirements:

$$a_x = A \cos(kz), k = 2\pi/l_z \quad (10)$$

where  $l_z$  is the box's height. In the simulation, the instantaneous  $V$  is defined as a Fourier coefficient:

$$V(t) = \frac{2 \sum_{i=1}^N m_i v_{i,x}(t) \cos[kr_{i,z}(t)]}{\sum_{i=1}^N m_i} \quad (11)$$

where  $m_i$  is the mass of an atom,  $r_{i,z}$  is the  $z$  coordinate, and  $v_{i,x}$  is the  $x$  component of the velocity. The amplitude of the velocity profile can be completely formed before measuring the average for  $V$ .

Four sample  $\text{CaCl}_2$  aqueous solutions' viscosities under an EF are shown in Figure 2. For comparison, the values in the absence of the EF are shown. As shown in Figure 2, the presence of  $\text{Fe}^{2+}$  increases the viscosity values in the  $\text{CaCl}_2$  system, and four typical aqueous  $\text{CaCl}_2$  solutions become viscous in the presence of  $\text{Fe}^{2+}$ . The EF also reduces the viscosity of aqueous  $\text{CaCl}_2$  solutions.

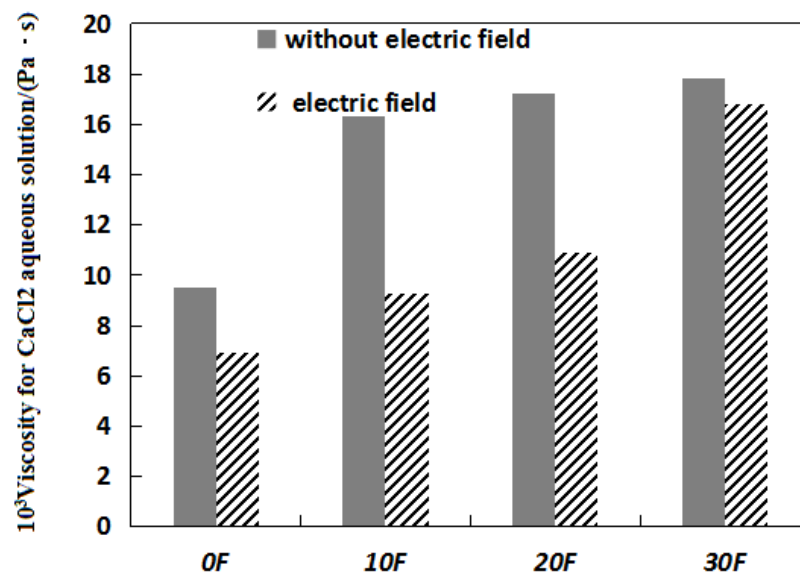


**Figure 2.** The  $10^3$  average viscosity with no  $\text{Fe}^{2+}$  ions added (0F) and 10  $\text{Fe}^{2+}$  added (10F), 20  $\text{Fe}^{2+}$  added (20F), and 30  $\text{Fe}^{2+}$  added (30F) with and without EF and EF.

The molecular weight of the particles inside the system is inversely proportional to the dynamic viscosity, which is a reflection of a sort of friction brought on by fluid motion

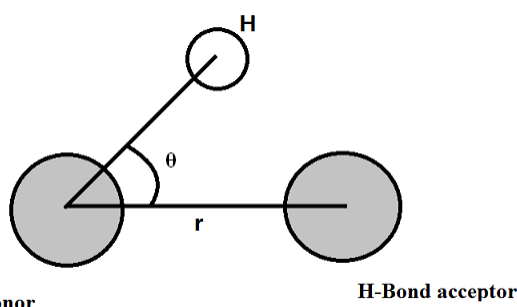
in the solution system. Bakker [45] found that viscosity is a distinct feature that describes the typical behavior of a large number of water molecules in aqueous solutions and that specific ions have a significant effect on the viscosity of water because of the extended lifetime of their initial hydration shells. Viscosity is substantially influenced by the water molecules' extended residence periods in ion hydration shells. The aqueous solution of  $\text{CaCl}_2$  also has no carbon–hydrogen bonds, making it an inorganic salt. Therefore, changes in the viscosity of  $\text{CaCl}_2$  solutions can be attributed to changes in the structural and kinetic properties of the water molecules.

Figure 2 demonstrates that without the EF, the viscosities of the four example  $\text{CaCl}_2$  aqueous solutions are  $9.49 \times 10^{-3}$  Pa·s,  $16.31 \times 10^{-3}$  Pa·s,  $17.24 \times 10^{-3}$  Pa·s, and  $17.81 \times 10^{-3}$  Pa·s. This means that the addition of  $\text{Fe}^{2+}$  can cause a relatively high viscosity in  $\text{CaCl}_2$  aqueous solutions. Dian et al. [46] studied  $\text{Ca}^{2+}$  solvation using polarizable atomic multipole potential, and their results show that the lifetime of water molecules in the first solvation shell of  $\text{Ca}^{2+}$  is 18 picoseconds (ps) when the temperature is 298 K. The experimental [47] values of the lifetime of water molecules in the first solvation shell of  $\text{Fe}^{2+}$  were determined in the range of  $10^5$ – $10^6$  ps when the temperature is 298.15 K, in contrast to only a few picoseconds for  $\text{Ca}^{2+}$ . Therefore, the addition of  $\text{Fe}^{2+}$  forms a water shell, which can lead to a longer residence time for water molecules in  $\text{Fe}^{2+}$  hydration shells compared to  $\text{Ca}^{2+}$ . Therefore, the viscosity of the solution is greatly increased by  $\text{Fe}^{2+}$ . Furthermore, the mobility of water molecules is related to the viscosity of the solution. According to Table 3, the activity of water molecules is more limited when the  $\text{Fe}^{2+}$  ion content increases, and this may result in a rise in the solution's viscosity.

Figure 2 demonstrates that when  $\text{Fe}^{2+}$  ions are available in the solution, the EF can reduce the viscosity of  $\text{CaCl}_2$  aqueous solutions. This is due to the fact that the EF reduces the mean dynamic residence time of water at  $\text{Ca}^{2+}$  and increases the activity of water molecules, both of which lead to a drop in dynamic viscosity. The viscosity of the salt solution can be reduced by the EF [48]. Electrostatic interaction between the water molecule and  $\text{Fe}^{2+}$  might raise the viscosity of the solution. This indicates that the dynamic viscosity of the  $\text{CaCl}_2$  solution can be reduced by the presence of  $\text{Fe}^{2+}$  and an external EF. In conclusion, the aqueous  $\text{CaCl}_2$  solution can become more viscous when  $\text{Fe}^{2+}$  ions are present, and the viscosity can be reduced when an EF is applied to an aqueous  $\text{CaCl}_2$  solution that contains  $\text{Fe}^{2+}$ . The decrease in viscosity of  $\text{CaCl}_2$  aqueous solutions, on the one hand, means that the scale-forming ions in the solution are reduced [40] and the fluidity of the solution is enhanced [49]. On the other hand, the decrease in the viscosity of  $\text{CaCl}_2$  aqueous solutions reduces the aggregation of calcium carbonate precipitates [41–43], which plays an effective role in anti-fouling. The decrease in solution viscosity reduces the adhesion of the electrode surface to ions and increases the rate of transport of oxidants, which can influence the capacitance values of the double layer and reflect changes in the surface state of the corrosion metal [36,37].

### 3.4. Effect of $\text{Fe}^{2+}$ and Electric Field on Hydrogen Bonds

The hydrogen bond network that is generated by water molecules has a significant impact on the precipitation of calcium carbonate [20,21] and is strongly connected to the chemical and physical characteristics of aqueous solutions [50,51]. The dissolution of calcium carbonate and corrosion products is influenced by the nature of the hydrogen bond network. According to Gromacs software, a hydrogen bond occurs when a donor and acceptor are separated by a van der Waals (VDW) length less than  $3.5\text{\AA}$  ( $r$ ) and when the hydrogen donor–acceptor angle is less than  $30^\circ$  [52]. The geometrical hydrogen bond requirement is displayed in Figure 3. The oxygen atoms in water molecules are the study's donors and acceptors. This work estimated the hydrogen bond angle as  $\angle \text{O}_D\text{-H}_D\text{-O}_A$  ( $\theta$ ), which is a suitable angle that is frequently used in the literature and offers helpful insight into the flexibility of donor hydrogen bonds [53]. Calculating the number of hydrogen bonds allows one to assess the overall importance of a hydrogen bond. The number of hydrogen bonds and the strength of the hydrogen bonds are positively correlated [52].



**Figure 3.** Geometrical hydrogen bond criterion.

The current study looked at both the number of hydrogen bonds ( $n_{HB}$ ) and the percentage of water molecules with  $n$  or more hydrogen bonds ( $f_n$ ). Without the addition of  $Fe^{2+}$  ( $0F$ ) and with the addition of 10  $Fe^{2+}$  ( $10F$ ), 20  $Fe^{2+}$  ( $20F$ ), and 30  $Fe^{2+}$  ( $30F$ ), the values of  $f_n$  and  $n_{HB}$  in  $CaCl_2$  aqueous solutions are shown in Table 4. ( $30F$ ). Additionally, the effect of the EF is demonstrated.

**Table 4.** The proportion of water molecules that have  $n$  hydrogen bonds ( $f_n$ ), the amount of  $Fe^{2+}$  that was added  $F(n^*F)$ , and the average number of hydrogen bonds per water molecule ( $n_{HB}$ ).

	Without Electrostatic Field				Under Electrostatic Field			
	$0F$	$10F$	$20F$	$30F$	$0F$	$10F$	$20F$	$30F$
$f_0(\%)$	58.09	61.54	62.20	65.02	57.99	60.93	61.10	64.08
$f_1(\%)$	31.17	29.75	29.16	28.39	31.08	29.88	29.80	29.36
$f_2(\%)$	8.23	7.37	7.30	6.59	8.34	7.80	7.70	7.04
$f_3(\%)$	1.56	1.29	1.28	1.18	1.63	1.34	1.36	1.27
$n_{HB}$	580.67	536.78	528.55	512.19	584.43	549.33	546.80	524.60

Table 4 demonstrates how the EF may alter the percentage of molecules without hydrogen bonds while increasing the percentage of molecules with one to three hydrogen bonds and the average number of hydrogen bonds in a water molecule, regardless of the presence or absence of  $Fe^{2+}$ . The proportion of water molecules with  $n$  or more hydrogen bonds might be used to define the dimension of the water cluster. For instance, the size of the water cluster increases with the proportion of molecules with two or three hydrogen bonds. The decrease in  $f_0$  and the rise in  $n_{HB}$ ,  $f_1$ ,  $f_2$ , and  $f_3$  indicate that water molecule activity is constrained and that more water molecules are shifting from the free state to the hydrogen-bonded state. This indicates that the EF improves the hydrogen structure of the water molecules to some extent. The findings in Table 4 further demonstrate that, regardless of whether the EF is administered or not,  $Fe^{2+}$  can enhance  $f_0$  and reduce  $n_{HB}$ ,  $f_1$ ,  $f_2$ , and  $f_3$ . Additionally, in the  $CaCl_2$  systems,  $n_{HB}$ ,  $f_1$ ,  $f_2$ , and  $f_3$  decrease as the amount of  $Fe^{2+}$  rises, whereas  $f_0$  increases. This is the result of the  $Fe^{2+}$  ion's ability to attract ion-dipole interactions, which retains water molecules in the ion hydration shell and reduces the number of water molecules bound by hydrogen bonds [54]. This results in fewer hydrogen bonds being created, an increase in the percentage of molecules without hydrogen bonds, a drop in the percentage of molecules with one to three hydrogen bonds, and a rise in the mean number of hydrogen bonds per water molecule.

#### 4. Conclusions

A methodical long-time balanced molecular dynamics simulation was used to examine the structural and dynamic characteristics of mixed solutions of  $CaCl_2$  and  $FeCl_2$  under an EF. Some significant findings were made.

- (1) Compared to  $Ca^{2+}$ , the hydrated structure of  $Fe^{2+}$  is more stable. The EF may raise the first water coordination number for  $Ca^{2+}$  and reduce the radius of hydrated  $Ca^{2+}$ . The EF has the ability to reduce the first water coordination number for hydrated  $Fe^{2+}$

- and expand its radius. The presence of  $\text{Fe}^{2+}$  has no discernible impact on the radius of hydrated  $\text{Ca}^{2+}$ ; however, it can lower the first water coordination number of  $\text{Ca}^{2+}$ .
- (2) The viscosity of  $\text{CaCl}_2$  in an aqueous solution can be efficiently raised by  $\text{Fe}^{2+}$ . The presence of an EF can make the mixed aqueous solution less viscous.
  - (3) The self-diffusion coefficient of  $\text{Ca}^{2+}$  can be lowered by  $\text{Fe}^{2+}$ .  $\text{Ca}^{2+}$ ,  $\text{Fe}^{2+}$ , and water molecules' self-diffusion coefficients can all be increased by an EF.
  - (4) An EF can enhance the hydrogen structure of the water molecules in the aqueous solution.

To sum up, the EF generated by an EAF system can change the structure of the solvent layer of  $\text{Ca}^{2+}$ , resulting in a reduction in the possibility of  $\text{Ca}^{2+}$  forming high-density calcite scale. In addition, the existence of an EF can also increase the activity of water molecules and reduce the viscosity of the solution, which will effectively hinder the release of  $\text{Fe}^{2+}$  in water and the formation of iron corrosion products.

**Author Contributions:** Conceptualization, methodology, software, and validation, Y.H.; data curation and writing—original draft preparation, B.W.; visualization and investigation, X.G.; supervision and writing—reviewing and editing, T.J. All authors have read and agreed to the published version of the manuscript.

**Funding:** This work was financially supported by the National Natural Science Foundation of China (No. 51408525), University Science and Technology Research Projects of Hebei Province (No. ZD2020324), The Central Guidance on Local Science and Technology Development Fund of Hebei Province (No. 216Z3601G), and the Natural Science Foundation of Hebei Province (No. E2022203061).

**Institutional Review Board Statement:** Not applicable.

**Informed Consent Statement:** Not applicable.

**Data Availability Statement:** Data sharing is not applicable to this article.

**Conflicts of Interest:** The authors declare no conflict of interest.

## References

1. Weiner, S.; Sagi, I.; Addadi, L. Choosing the crystallization path less traveled. *Science* **2005**, *309*, 1027–1028. [[CrossRef](#)] [[PubMed](#)]
2. Qi, J.Q.; Guo, R.; Wang, Y.; Liu, X.W.; Chan, H.L.W. Electric field-controlled crystallizing  $\text{CaCO}_3$  nanostructures from solution. *Nanoscale Res. Lett.* **2016**, *11*, 120. [[CrossRef](#)] [[PubMed](#)]
3. Li, H.H.; Liu, Z.F.; Gao, Y.H.; Zhang, L.H.; Li, X.H. Influence of electrostatic water treatment on crystallization behavior of  $\text{CaCO}_3$  and synergistic scale inhibition with a green scale inhibitor. *CIESC J. Chem. Ind. Eng.* **2013**, *64*, 1736–1742. [[CrossRef](#)]
4. Lin, D.; Dai, N.; Chen, Y.; Ni, Q.; Zhang, X.; Zhang, J. Effect of direct current electric field on initial corrosion of steel exposed to simulated marine environment. *Corros. Sci. Protection Technol.* **2017**, *29*, 63–67. [[CrossRef](#)]
5. Sarin, P.; Snoeyink, V.L.; Lytle, D.A.; Kriven, W.M. Iron corrosion scales: Model for scale growth, iron release, and colored water formation. *J. Environ. Eng.* **2004**, *130*, 364–373. [[CrossRef](#)]
6. Finan, M.A.; Harris, A.; Marshall, A. Ecologically acceptable method of preventing corrosion/scale problems by control of water conditions. *Natl. Assoc. Corros. Eng.* **1980**, *204*, 24–29.
7. de Leeuw, N.H. Molecular dynamics simulations of the growth inhibiting effect of  $\text{Fe}^{2+}$ ,  $\text{Mg}^{2+}$ ,  $\text{Cd}^{2+}$ , and  $\text{Sr}^{2+}$  on calcite crystal growth. *J. Phys. Chem. B* **2002**, *106*, 5241–5249. [[CrossRef](#)]
8. Zhao, G.-J.; Liu, J.-Y.; Zhou, L.-C.; Han, K.-L. Site-selective photoinduced electron transfer from alcoholic solvents to the chromophore facilitated by hydrogen bonding: A new fluorescence quenching mechanism. *J. Phys. Chem. B* **2007**, *111*, 8940–8945. [[CrossRef](#)]
9. Zhao, G.J.; Han, K.L. Hydrogen bonding in the electronic excited state. *Accounts. Chem. Res.* **2012**, *45*, 404. [[CrossRef](#)]
10. Chen, J.S.; Yuan, M.H.; Wang, J.P.; Yang, Y.; Chu, T.S. Sensing mechanism for biothiols chemosensor DCO: Roles of excited-state hydrogen-bonding and intramolecular charge transfer. *J. Phys. Chem. A* **2014**, *118*, 8986–8995. [[CrossRef](#)]
11. Zhu, L.; Han, Y.; Zhang, C.; Zhao, R.; Tang, S. Molecular dynamics simulation for the impact of an electrostatic field and impurity  $\text{Mg}^{2+}$  ions on hard water. *RSC Adv.* **2017**, *7*, 47583. [[CrossRef](#)]
12. Nedyalkova, M.; Madurga, S.; Pisov, S.; Pastor, I.; Vilaseca, E.; Mas, F. Molecular dynamics simulation of the spherical electrical double layer of a soft nanoparticle: Effect of the surface charge and counterion valence. *J. Chem. Phys.* **2012**, *137*, 174701. [[CrossRef](#)] [[PubMed](#)]
13. Li, M.; Duan, Z.; Zhang, Z.; Zhang, C.; Weare, J. The structure, dynamics and solvation mechanisms of ions in water from long time molecular dynamics simulations: A case study of  $\text{CaCl}_2$  (Aq) aqueous solutions. *Mol. Phys.* **2008**, *106*, 2685–2697. [[CrossRef](#)]

14. Chialvo, A.A.; Simonson, J.M. The structure of CaCl<sub>2</sub> aqueous solutions over a wide range of concentration. Interpretation of diffraction experiments via molecular simulation. *J. Chem. Phys.* **2003**, *119*, 8052–8061. [[CrossRef](#)]
15. Isele-Holder, R.E.; Mitchell, W.; Ismail, A.E. Development and application of a particle-particle particle-mesh ewald method for dispersion interactions. *J. Chem. Phys.* **2012**, *137*, 174107. [[CrossRef](#)] [[PubMed](#)]
16. Gunsteren, W.F.V.; Billeter, S.R.; Eising, A.A.; Hünenberger, P.H.; Krüger, P.K.H.C.; Mark, A.E.; Scott, W.R.P.; Tironi, I.G. *Biomolecular Simulation: The GROMOS96 Manual and User Guide*; Vdf Hochschulverlag AG an der ETH Zürich: Zürich, Switzerland, 1996; Volume 86, pp. 1–1044.
17. Duarte, F.; Bauer, P.; Barrozo, A.; Amrein, B.A.; Purg, M.; Åqvist, J.; Kamerlin, S.C.L. Force field independent metal parameters using a nonbonded dummy model. *J. Phys. Chem. B* **2014**, *118*, 4351–4362. [[CrossRef](#)] [[PubMed](#)]
18. Han, Y.; Zhao, Y. Influence to the structure and dynamics of hydrated Ca<sup>2+</sup> and water molecules in CaCl<sub>2</sub> aqueous solution caused by external AC electric field: A mechanism study by molecular dynamics simulation. *Int. J. Electrochem. Sci.* **2012**, *7*, 10008–10026.
19. Lopez-Berganza, J.A.; Diao, Y.; Pamidighantam, S.; Espinosa-Marzal, R.M. Ab initio studies of calcium carbonate hydration. *J. Phys. Chem. A* **2015**, *119*, 11591–11600. [[CrossRef](#)]
20. Raiteri, P.; Gale, J.D. Water is the key to nonclassical nucleation of amorphous calcium carbonate. *J. Am. Chem. Soc.* **2010**, *132*, 17623–17634. [[CrossRef](#)]
21. Dorvee, J.R.; Veis, A. Water in the formation of biogenic minerals: Peeling away the hydration layers. *J. Struct. Biol.* **2013**, *183*, 278–303. [[CrossRef](#)]
22. York, D.M.; Darden, T.A.; Pedersen, L.G.; Anderson, M.W. Molecular dynamics simulation of HIV-1 protease in a crystalline environment and in solution. *Biochemistry* **1993**, *32*, 3196. [[CrossRef](#)]
23. Ye, Q.; Chen, X.; Zhou, J.; Zhao, H.F.; Chu, W.S.; Zheng, X.S.; Marcelli, A.; Wu, Z.Y. Local hydrated structure of an Fe<sup>2+</sup>/Fe<sup>3+</sup> aqueous solution: An investigation using a combination of molecular dynamics and X-ray absorption fine structure methods. *Chin. Phys. C* **2013**, *37*, 118–123. [[CrossRef](#)]
24. Han, Y.; Zhu, L.; Zhang, Y. Molecular dynamics simulation for the impact of external electric fields on CaCl<sub>2</sub> aqueous solution. *Chem. Res. Chin. Univ.* **2016**, *32*, 641–646. [[CrossRef](#)]
25. Cunningham, A.B.; Phillips, A.J.; Troyer, E.; Lauchnor, E.; Hiebert, R.; Gerlach, R.; Spangler, L. Wellbore leakage mitigation using engineered biomineralization. *Energy Procedia* **2014**, *63*, 4612–4619. [[CrossRef](#)]
26. Yang, Q.; Liu, Y.; Gu, A.; Ding, J.; Shen, Z. Investigation of calcium carbonate scaling inhibition and scale morphology by AFM. *J. Colloid. Interf. Sci.* **2001**, *240*, 608–621. [[CrossRef](#)] [[PubMed](#)]
27. Han, Y.; Zhang, C.; Wu, L.; Zhang, Q.; Zhu, L.; Zhao, R. Influence of alternating electromagnetic field and ultrasonic on calcium carbonate crystallization in the presence of magnesium ions. *J. Cryst. Growth* **2018**, *499*, 67–76. [[CrossRef](#)]
28. Floris, F.; Persico, M.; Tani, A.; Tomasi, J. Ab Initio effective pair potentials for simulations of the liquid state, based on the polarizable continuum model of the solvent. *Chem. Phys. Lett.* **1992**, *199*, 518–524. [[CrossRef](#)]
29. Busch, K.W.; Busch, M.A.; Parker, D.H.; Darling, R.E.; McAtee, J.L. Studies of a water treatment device that uses magnetic fields. *Corrosion* **1986**, *42*, 211–221. [[CrossRef](#)]
30. Tsuzuki, S.; Shinoda, W.; Saito, H.; Mikami, M.; Tokuda, H.; Watanabe, M. Molecular dynamics simulations of ionic liquids: Cation and anion dependence of self-diffusion coefficients of ions. *J. Phys. Chem. B* **2009**, *113*, 10641–10649. [[CrossRef](#)]
31. Henritzi, P.; Bormuth, A.; Klameth, F.; Vogel, M. A molecular dynamics simulations study on the relations between dynamical heterogeneity, structural relaxation, and self-diffusion in viscous liquids. *J. Chem. Phys.* **2015**, *143*, 164502. [[CrossRef](#)]
32. Fischler, M.A.; Bolles, R.C. Random sample consensus: A paradigm for model fitting with applications to image analysis and automated cartography. *Commun. Assoc. Comput.* **1981**, *24*, 381. [[CrossRef](#)]
33. Guo, B.; Han, H.; Chai, F. Influence of magnetic field on microstructural and dynamic properties of sodium, magnesium and calcium ions. *Trans. Nonferrous Met. Soc. China* **2011**, *21*, s494–s498. [[CrossRef](#)]
34. Wei, S.; Zhong, C.; Su-Yi, H. Molecular dynamics simulation of liquid water under the influence of an external electric field. *Mol. Simulat.* **2005**, *31*, 555–559. [[CrossRef](#)]
35. Bruneval, F.; Donadio, D.; Parrinello, M. Molecular dynamics study of the solvation of calcium carbonate in water. *J. Phys. Chem. B* **2007**, *111*, 12219–12227. [[CrossRef](#)]
36. Ying, T.Y.; Yang, K.L.; Yiaccoumi, S.; Tsouris, C. Electro sorption of ions from aqueous solutions by nanostructured carbon aerogel. *J. Colloid. Interf. Sci.* **2002**, *250*, 18–27. [[CrossRef](#)]
37. Morimoto, T.; Hiratsuka, K.; Sanada, Y. Development and current status of electric double-layer capacitors. *MRS Proc.* **1995**, *393*, 397. [[CrossRef](#)]
38. Chen, L.; Zhang, H.; Qi, Z.-P.; Yao, W.; Wan, J.-J.; Shao, M.; Zhang, C.-C. Synthesis of calcium carbonate crystals by using bacteria. *Synth. React. Inorg. Met. Nano-Metal Chem.* **2012**, *42*, 972–975. [[CrossRef](#)]
39. Pach, L.; Hrabe, Z.; Komarneni, S.; Roy, R. Controlled crystallization of vaterite from viscous solutions of organic colloids. *J. Mater. Res.* **1990**, *5*, 2928–2932. [[CrossRef](#)]
40. Ricciardiello, F.; Roitti, S. The corrosion of Fe and Ag in S liquid at lowtemperature. Effect of S viscosity. *Corros. Sci.* **1972**, *12*, 651–659. [[CrossRef](#)]
41. Jada, A.; Verraes, A. Preparation and microelectrophoresis characterisation of calcium carbonate particles in the presence of anionic polyelectrolyte. *Colloids Surf. A Physicochem. Eng. Asp.* **2003**, *219*, 7–15. [[CrossRef](#)]

42. Domingo, C.; García-Carmona, J.; Loste, E.; Fanovich, A.; Fraile, J.; Gómez-Morales, J. Control of calcium carbonate morphology by precipitation in compressed and supercritical carbon dioxide media. *J. Cryst. Growth* **2004**, *271*, 268–273. [[CrossRef](#)]
43. Xie, A.J.; Zhang, C.Y.; Shen, Y.H.; Qiu, L.-G.; Xiao, P.P.; Hu, Z.Y. Morphologies of calcium carbonate crystallites grown from aqueous solutions containing polyethylene glycol. *Cryst. Res. Technol.* **2006**, *41*, 967–971. [[CrossRef](#)]
44. Hess, B. Determining the shear viscosity of model liquids from molecular dynamics simulations. *J. Chem. Phys.* **2002**, *116*, 209. [[CrossRef](#)]
45. Bakker, H.J. Structural dynamics of aqueous salt solutions. *Chem. Rev.* **2008**, *108*, 1456–1473. [[CrossRef](#)] [[PubMed](#)]
46. Jiao, D.; King, C.; Grossfield, A.; Darden, T.A.; Ren, P. Simulation of  $\text{Ca}^{2+}$  and  $\text{Mg}^{2+}$  solvation using polarizable atomic multipole potential. *J. Phys. Chem. B* **2006**, *110*, 18553–18559. [[CrossRef](#)]
47. Ohtaki, H.; Radnai, T. Structure and dynamics of hydrated ions. *Chem. Rev.* **1993**, *93*, 1157–1204. [[CrossRef](#)]
48. Han, G.; Fang, Z.; Chen, M. Modified Eyring viscosity equation and calculation of activation energy based on the liquid quasi-lattice model. *Sci. China Phys. Mech. Astron.* **2010**, *53*, 1853–1860. [[CrossRef](#)]
49. Ravi, K.R.; Pillai, R.M.; Amaranathan, K.R.; Pai, B.C.; Chakraborty, M. Fluidity of aluminum alloys and composites: A review. *J. Alloy. Compd.* **2008**, *456*, 201–210. [[CrossRef](#)]
50. Lee, W.J.; Chang, J.G.; Ju, S.P. Hydrogen-Bond structure at the interfaces between Water/Poly(Methyl Methacrylate), Water/Poly(Methacrylic Acid), and Water/Poly(2-Aminoethylmethacrylamide). *Langmuir* **2010**, *26*, 12640–12647. [[CrossRef](#)]
51. Pan, Z.; Chen, J.; Lü, G.; Geng, Y.Z.; Zhang, H.; Ji, Q. An Ab initio molecular dynamics study on hydrogen bonds between water molecules. *J. Chem. Phys.* **2012**, *136*, 164313. [[CrossRef](#)]
52. Li, Y.X.; Wei, Z.D.; Zhao, Q.L.; Ding, W.; Zhang, Q.; Chen, S.G. Preparation of Pt/Graphene catalyst and its catalytic performance for oxygen reduction. *Acta. Phys-Chim. Sin.* **2011**, *27*, 858–862. [[CrossRef](#)]
53. Lee, H.-S.; Tuckerman, M.E. Structure of liquid water at ambient temperature from ab initio molecular dynamics performed in the complete basis set limit. *J. Chem. Phys.* **2006**, *125*, 154507. [[CrossRef](#)] [[PubMed](#)]
54. Karmakar, A.; Choudhuri, J.R.; Yadav, V.K.; Mallik, B.S.; Chandra, A. A first principles simulation study of vibrational spectral diffusion in aqueous NaBr solutions: Dynamics of water in ion hydration shells. *Chem. Phys.* **2013**, *412*, 13–21. [[CrossRef](#)]